ADVANCED OPTICAL MATERIALS
www.advopticalmat.de

Hot-Spot Engineering Through Soft Actuators for Surface-Enhanced Raman Spectroscopy (SERS) Applications

*Gorkem Liman, Emrecan Yildiz, Hasan Ilhan, Arif E. Cetin, and Gokhan Demirel**

Surface-enhanced Raman spectroscopy (SERS) is a powerful analytical tool to detect molecular species at ultralow concentrations. However, considering current approaches, controlling and tuning plasmonic hot-spot formations where the Raman signal enhancements maximize are still challenging due to high process cost, complexity, and inability of large-area fabrication. To address these problems, a strategy is demonstrated based on the controlled folding of polymeric materials, which is a new perspective in the field of SERS. Manipulation of hot-spot formations through controlled polymer folding enables a Raman signal enhancement up to 70 folds for the probe methylene blue molecule. Furthermore, sample collection and analysis have been successfully implemented through the magnetic field control of the platform motion and folding manipulation. The results demonstrate that soft actuator platforms can bring new modalities in sensing applications.

1. Introduction

Molecular detection at ultralow concentrations has emerged as one of the most appealing research area in recent years.[1–5] Conventional techniques for the analysis of molecular species could be based on varying methodologies including electrical,[6] optical,[7] and vibrational.[8] Due to the ability of non-destructive analysis with unique selectivity, surface-enhanced Raman spectroscopy (SERS) is considered as a prominent tool for molecular detection.[9,10] Over the past decade, a large variety of SERS based sensing platforms have been developed employing plasmonic materials,[11] inorganic semiconductors,[12] and organic semiconductors[13,14] for variety of applications, e.g., environmental protection,[15] food safety,[16] and homeland security.[17] The enhancement mechanism in SERS mainly relies on the electrical field magnification through the excitation of localized surface plasmon resonances of the underlying SERS-active materials.[11] These localized regions of highly intense local electric fields are called as "Hot-Spots." Although the formation of dense hot-spots in SERS platforms provides high Raman signal enhancements, small interparticle distances (<10 nm) between the plasmonic structures should be realized.[10] Formation of hot-spots for SERS applications can be manipulated through different approaches, which are called as "Plasmonic Hot-Spot Engineering."[18,19] Traditional hot-spot engineering tools are fundamentally classified into two classes—bottom-up and top-down approaches.[20] Bottom-up techniques employ nanoparticles with plasmonic features. However, in these techniques, the uncontrolled aggregation of nanoparticles, insufficient strength of resulting hot-spots for sensing, and limited SERS active area lead to inconsistent field enhancement and SERS signals.[18] To overcome these problems, the top-down approaches, which mainly rely on lithography techniques (e.g., e-beam and focus ion beam), have been proposed to control hot-spot formations.[18] Although the interparticle distance and structural geometries can be precisely tuned with the use of these ways, they are technologically demanding and quite expensive in the fabrication of large quantities of substrates. Therefore, alternative approaches for "Plasmonic Hot-Spot Engineering" are of great interest not only to widen SERS applications but also to further elucidate fundamental questions.

Controlling the formation of plasmonic hot-spots, which serve as the key factor in collecting high and reliable Raman signals from the analyte molecules, is critical in SERS applications. Unfortunately, current approaches encounter great limitations in controlling and tuning these formations such as high process cost and inability of large-area fabrication. In this context, foldable platforms offer unique possibilities for SERS applications. For example, Gracias and co-workers developed a technique called mechanical trap surface-enhanced Raman spectroscopy (MTSERS) using a foldable platform.[21] They demonstrated that the fabricated foldable platform allows to capture and encapsulate target cells, while providing a stable orientation for 3D-SERS imaging. In another work, Xu et al. also reported a foldable 3D-SERS sensing platform which is capable of conformally wrapping a target sample.[22] Considering these advancements in the literature on foldable platforms, most focus on capturing or trapping targeted materials, while folding process does not contribute to the hot-spot formations. These works bring a question how foldable platforms could be used to control hot-spot formations to enhance the Raman signal intensities.

In this article, we proposed a strategy based on the controlled-folding of polymeric materials to manipulate hot-spot formations

G. Liman, E. Yildiz, Dr. H. Ilhan, Prof. G. Demirel
Bio-inspired Materials Research Laboratory (BIMREL)
Department of Chemistry
Gazi University
Ankara 06500, Turkey
E-mail: nanobiotechnology@gmail.com
Prof. A. E. Cetin
Izmir Biomedicine and Genome Center
Balcova, Izmir 35340, Turkey
The ORCID identification number(s) for the author(s) of this article can be found under https://doi.org/10.1002/adom.202100009.

DOI: 10.1002/adom.202100009

as a new perspective in the field of SERS. Manipulation of hot-spot formations through controlled polymer folding led to an amplification within the localized electromagnetic field that could result in stronger SERS signals compared to classical plasmonic geometries. Using this technique, we also introduced an ability for polymeric platforms to control their motion with a simple modification, which could dramatically facilitate the sampling and analysis of target molecules in the desired environment.

2. Results and Discussion

In our investigations, pre-strained polystyrene (PS) sheets (≈0.3 mm thickness) were chosen as the starting material. Controlled folding of the pre-strained PS sheets with colored hinges using a light source has been previously reported in the literature.[23–25] As these materials absorb light, temperature of the colored areas increases due to the heat generated by the light. However, folding does not occur until reaching the glass transition temperature of the polymer (≈102 °C).[25] For such materials, the desired 3D geometry can be easily obtained from 2D polymer sheets by controlling temperature distribution on the material by varying hinge geometries or colors.[24] In this work, PS sheets were first designed by a computer to have different hinge widths (0.5–4.5 mm) and colors (black, yellow, red, and green), i.e., they could exhibit the desired level of folding for further engineering the plasmonic hot-spot formations (Figure S1, Supporting Information). Designs (1 cm × 3 cm) were then transferred to polymer sheets using a laser printer. The platforms with different colored hinges were exposed to different light sources (IR (250 watt), blue, red, and green LEDs (50 watt)) (Figures S2–S5, Supporting Information). The distance between light source and the platform was kept constant at ≈2 cm for 50 W LEDs and ≈8 cm for IR lamp. Depending on the hinge widths/colors and light source, polymeric platforms exhibit different folding behaviors. For platforms with black color hinges (**Figure 1**a), folding angle was about 42.5° under blue light illumination when the hinge width was 0.5 mm (Figure 1b). At 1.5 mm hinge width, folding angle was reached to 72.6°. Folding was completed (180°) when the hinge width was 4.5 mm. We also analyzed the folding time for the platforms with 2.0 mm hinge width. For these designs, folding

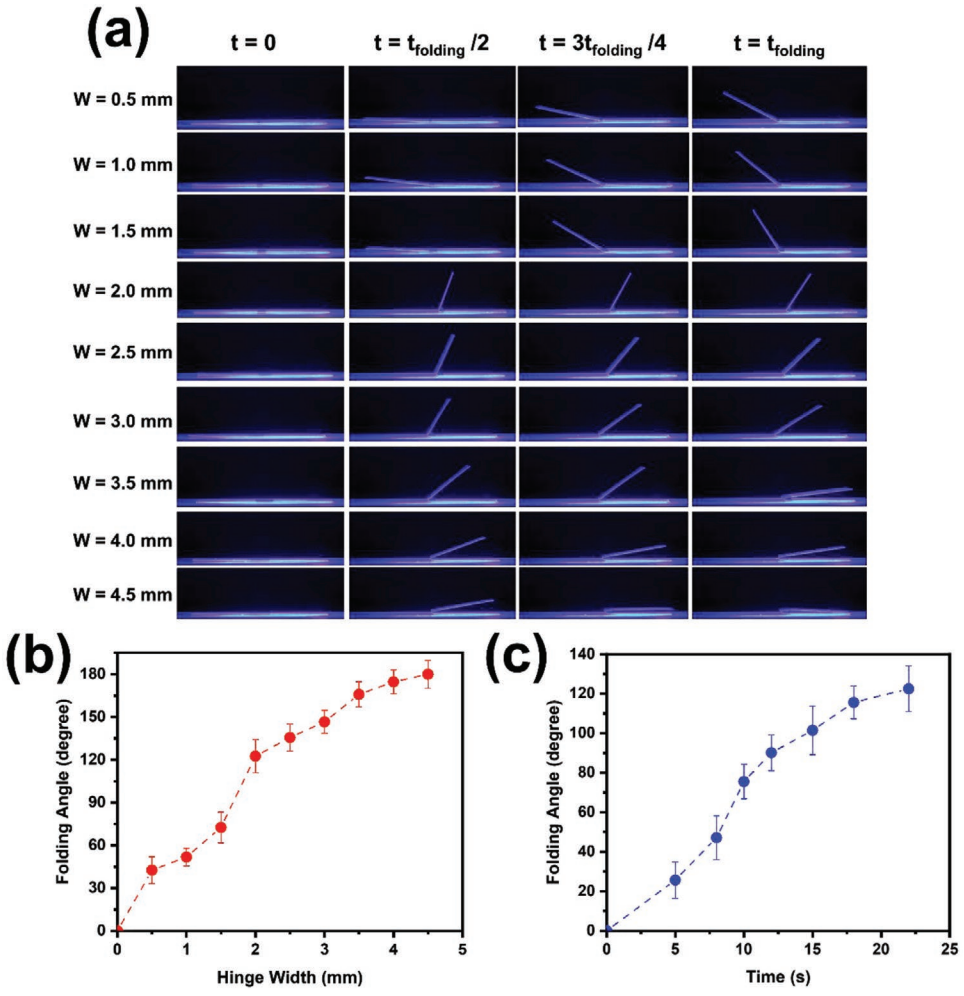

Figure 1. a) Optical images of 2D PS polymeric platforms with different black colored hinge widths (W = 0.5–4.5 mm) under blue LED light illumination (50 watt). b) Folding angles of 2D PS platforms as a function of hinge width and c) folding angles of 2D PS platforms with a 2.0 mm hinge width as a function of time.

was started at ≈5 s, and reached ≈122° of folding angle at ≈22 s (Figure 1c). In the light of these results, it was determined that polymeric platforms with 2.0 mm hinge width fabricated with black ink were chosen for further studies, which were folded using blue light at the desired level.

In the next step, control and manipulation studies for hot-spot formations were investigated using polymeric platforms. The key point in hot-spot formation is to control the distance between plasmonic structures.[18,20] To this end, gold nanostructures (AuNPs) with a diameter of ≈20 nm were first synthesized as a model plasmonic particle (Figure S6, Supporting Information). Two different polymeric platforms, e.g., two-arms and three-arms, were designed and fabricated for hot-spot manipulation studies. When these 2D designs with AuNPs are folded, they will form pyramid-like geometries, and the distance between plasmonic structures maximize the intensity of localized electromagnetic fields by bringing the arms close to each other (Movie S1 and S2, Supporting Information). In the designs, black ink was used based on the information obtained from the studies mentioned above, and blue LED light was preferred to generate heat on the polymeric sheets. Synthesized plasmonic nanoparticles were decorated on the arms of the designs before light illumination. For this purpose, polymeric platforms were first modified with a polydopamine (PDOP) layer using a mask in order to bond nanoparticles homogeneously and chemically on the polymeric surfaces. PDOP layers were used to have a certain thickness based on the oxidative polymerization of dopamine molecules.[26,27] In our previous studies, we demonstrated that ≈10 nm PDOP film thickness is sufficient for AuNPs to adhere on the surface.[28,29] Therefore, PDOP film thickness for all platforms was kept constant at ≈10 nm. After the PDOP films were formed on the platforms, the AuNPs were decorated on the arms to have different particle densities. Nanoparticle density on the arms of the designs was controlled by changing the retention time (3–24 h). Scanning electron microscopy (SEM) images of the fabricated films are given in **Figure 2**a–c. Here, for 3 h retention time, nanoparticle density on the surface was found as 2.24×10^{10} nanoparticles per cm^2, while it increased to 5.72×10^{10} nanoparticles per cm^2 for 24 h retention time. However, the retention time was increased more than 24 h, uncontrolled AuNP aggregations were observed on the surfaces, i.e., it was not used in our study (Figure S7, Supporting Information). The AuNP modified platforms were also characterized by UV–vis. As-synthesized nanoparticles exhibit an absorbance maximum at 520 nm, whereas this peak was shifted to 561 nm for 3 h, 576 nm for 12 h, and 627 nm for 24 h retention time (Figure 2d). UV–vis spectrum of the folded two-arms platforms was also evaluated and indicated that there is only a minor LSPR change from 627 to 671 nm after folding (Figure S8, Supporting Information).

Folding ability of two-arms and three-arms platforms modified with AuNPs were subsequently examined. In Figure 2, optical images before and after the folding, and SEM images of the folded samples are given. The images clearly show that both designs formed a pyramid-like geometry by folding their arms along the desired directions (Figure 2g,j). After the targeted folding geometries were obtained for both designs, their abilities to form hot-spots was investigated in detail using SERS. In our study, methylene blue (MB) was selected as the Raman probe due to its well-known characteristic Raman bands and, more importantly, not exhibiting an optical transition at the Raman laser excitation energy (1.58 eV) employed in this work neither in solution nor in the solid state (onset absorption energy for MB = 1.78–1.65 eV) (Figure S9, Supporting Information).[13,14] Therefore, the contribution of the probe molecule's resonant excitation to Raman enhancement could be excluded. In each test, a 5.0 µL of 10^{-3} M aqueous MB solution was first dropped on one arm of both designs containing different AuNPs densities, where SERS analysis were conducted after the evaporation of the solvent. First, MB Raman spectra were obtained before the platforms were folded. Several prominent bands originating from MB molecules were detected at 448 cm^{-1} for (C–N–C) skeletal stretching, 1181 cm^{-1} for (C–N) stretching, 1394 cm^{-1} for in-plane (C–H) ring deformation, and 1620 cm^{-1} for (C–C) ring stretching (**Figure 3**a,b). Increase in the nanoparticle density for both designs led an enhancement for Raman features in the spectra of MB molecules. Here, it is important to note that underlying PDOP coated PS platforms have intrinsic Raman spectrum with a low peak intensity. However, when we applied MB on the platforms, the background signals from PS and PDOP were discarded due to high Raman cross-section of MB (Figure S10, Supporting Information). After folding of the designed platforms, there was a significant increment in the formation of hot-spots; as a result, a dramatic signal enhancement was determined within the Raman peaks observed in the spectrum. The (C–N–C) skeletal stretching peak signal observed at 448 cm^{-1} increased by 8.3 folds for two-arms platforms obtained with 3 h AuNP modification after folding compared to unfolded platforms, while such increase was found as 9.6 folds for three-arms platforms (Figure 3c). For 12 h AuNP modified platforms, a 61.5 folds enhancement was observed for the two-arms design compared to the unfolded platforms. This signal enhancement for the same peak was determined as 24.5 folds for three-arms designs. Signal enhancement has been maximized when AuNPs were modified for 24 h. For the peak at 448 cm^{-1}, signal enhancements were found as 69.7 and 25.1 folds for two- and three-arms designs compared to the unfolded ones. Similar signal enhancements were observed for all characteristic peaks of MB (Figure 3d–f; Table S1, Supporting Information). In addition to these investigations, reproducibility of the fabricated platforms was evaluated. We collected SERS spectra of MB using 24 h AuNP deposited two-arms platforms after folding from three randomly selected positions at joint for four different samples under the same experimental conditions (Figure S11, Supporting Information). For all platforms, similar Raman spectra were determined with high reproducibility. To clarify and quantify the reproducibility, we calculated relative standard deviation (RSD) value of the Raman band at 1620 cm^{-1} for the spectra given in Figure S11 in the Supporting Information. The calculated RSD value (<0.21) and peak positions indicated the good SERS signal reproducibility for fabricated platforms.

In order to understand the hot-spot formations, SERS spectra of MB were obtained from different points of the two-arms designs after folding. In **Figure 4**(I), SERS spectra are given for MB collected from different points starting from a spot ≈1.0 mm away from to the joint point of the folded structure. In our experiments, the platforms were placed parallel to the microscope stage as shown in Figure S12 in the Supporting

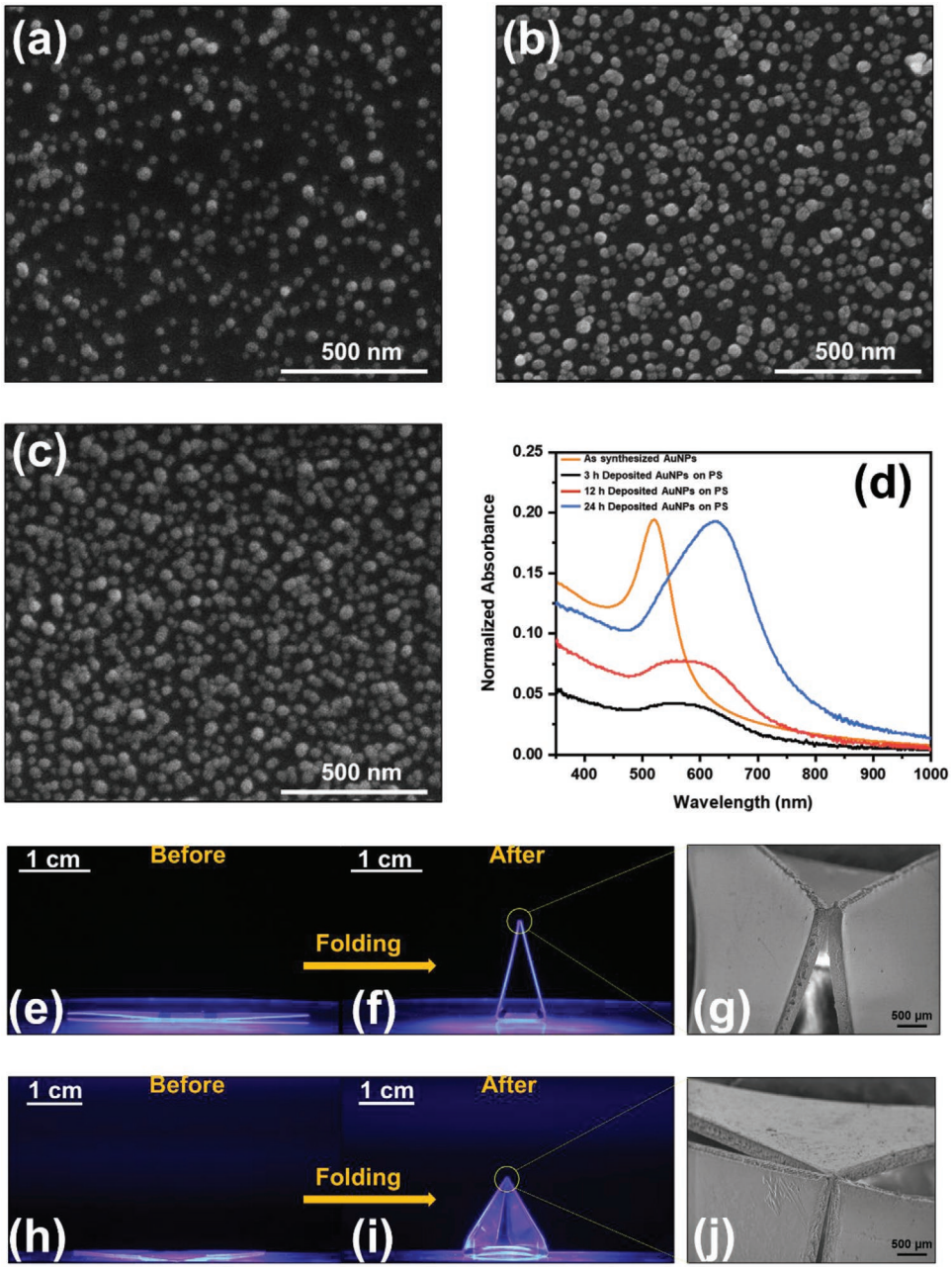

Figure 2. SEM images of AuNP decorated 2D PS platforms for a) 3 h, b) 12 h, and c) 24 h of retention time periods. d) UV–vis spectra of AuNP decorated 2D PS platforms with different retention time periods. The optical and SEM images of e–g) two-arms and h–j) three-arms polymeric platforms under blue LED illumination.

Information. Therefore, the incident angle of the Raman laser with respect to samples was about 40° instead of 90°. The SERS spectrum collected from point "A" revealed very low signal intensities for the analyte molecule similar to the unfolded designs (92 vs 98 counts for 448 cm^{-1} and 447 vs 598 counts for 1620 cm^{-1}). At this point, folding does not contribute to plasmonic hot-spot formation due to the large distance between plasmonic particles on different arms. The collected SERS spectrum mainly results from the interaction of nanoparticles on the same arms with each other. At point "B" (≈0.3 mm to the end point), a small increment in the Raman signal was observed (≈approximately sevenfolds for 448 cm^{-1} peak, and approximately fourfolds for 1620 cm^{-1} peak). However, for point "C" (≈0.1 mm to the joint point), the particles in both arms came to a much closer distance due to the folding of the platform, i.e., they resulted in a signal enhancement of ≈22 folds for 448 cm^{-1}, and ≈15 folds for 1620 cm^{-1} over the unfolded platform. A significant signal enhancement was observed at point "D" (the joint point). Due to the intense hot-spot formations at the "D", signal enhancement has reached to ≈70 folds. In order to substantiate our claims, we investigated folded platforms with a Jasco NRS-4500 Confocal Raman Microscope with

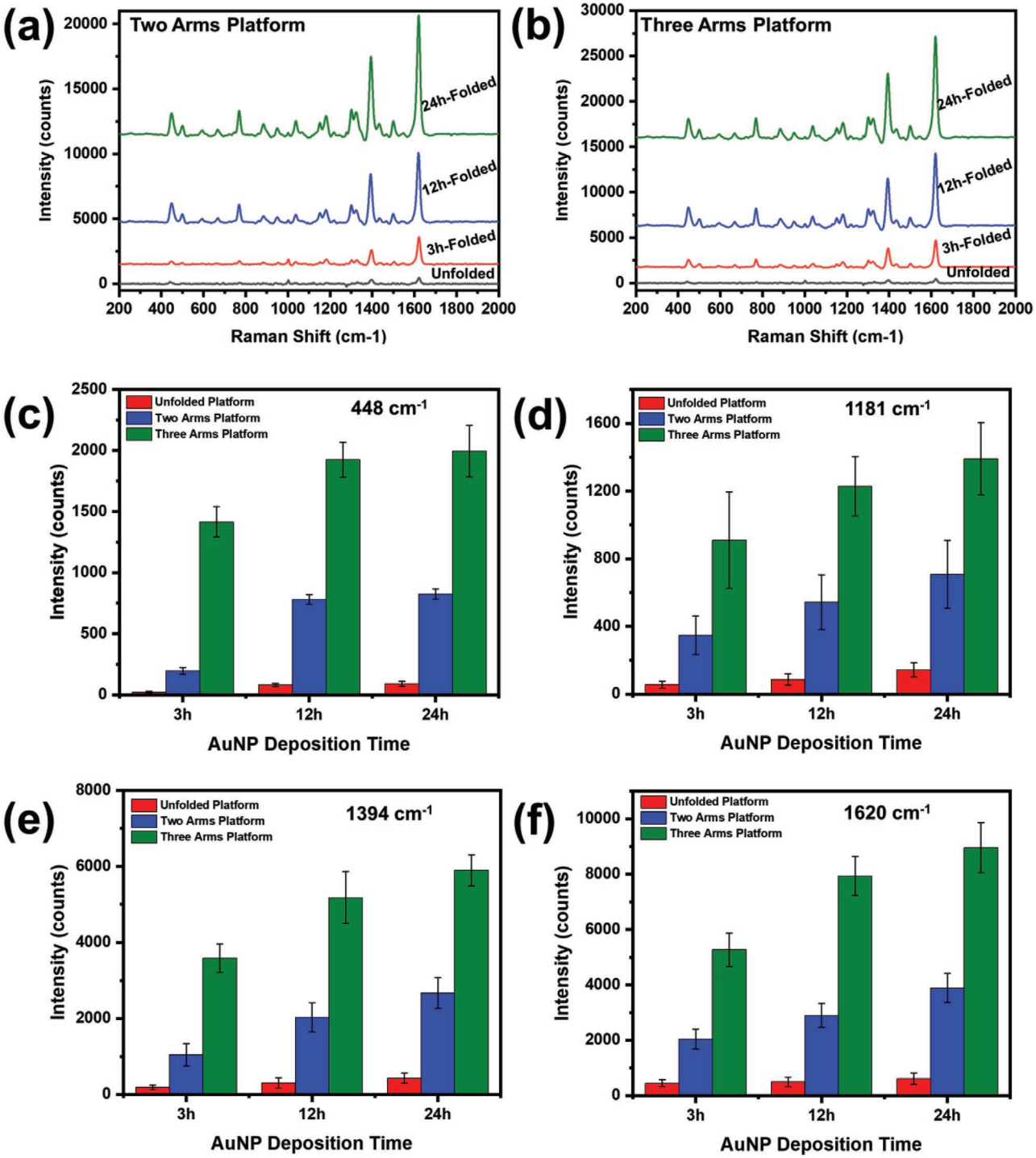

Figure 3. SERS spectra of MB collected from a) two-arms and b) three-arms polymeric platforms having different densities of Au NPs on arms before and after folding. c–f) Raman intensity histograms of 448, 1181, 1394, and 1620 cm^{-1} peaks derived from SERS spectra in (a) and (b). (For all experiments, the concentration of MB was 10^{-3} M).

a mapping software (785 nm laser, 10× objective) (Figure 4(II)). Mapping process was performed from outside of the contact point of platforms to the center of the contact by collecting more than 1000 Raman spectra. As expected, MB Raman signals (448 and 1620 cm^{-1}) gradually increased from outside of the contact point to the center of the contact point, indicating a clear hot-spot engineering. The Raman spatial mapping of 1620 and 448 cm^{-1} MB peaks for the folded two-arms platforms at different planes along the *z*-axis (Figure S13, Supporting Information) also showed that Raman signal intensities for both peaks in the *z*-plane Raman maps with stronger intensities at the joint point. The resultant spatial map indicates that hot-spot

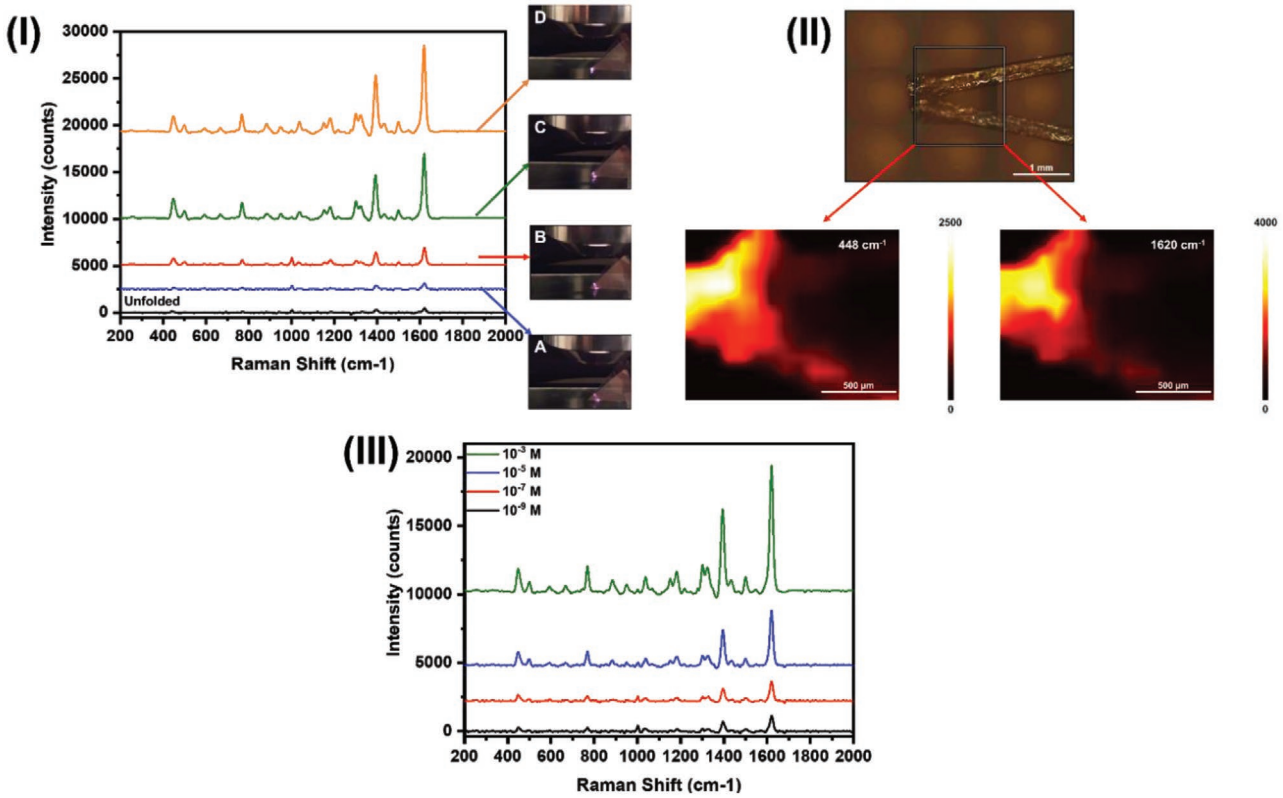

Figure 4. (I) SERS spectra of MB (10^{-3} M) acquired from folded two-arms polymeric platforms from different points. (II) SERS Raman mapping of folded two-arms polymeric platforms for 1620 and 448 cm^{-1} peaks of MB. (III) SERS spectra of MB collected from folded two-arms polymeric platforms at different concentrations.

formations are denser towards the center of the joint as compared to the other areas. These observations indicate that SERS signal enhancement could be simply manipulated through the controlling the polymer folding.

Control and manipulation of hot-spot formations by polymer folding does not only enhance the Raman signals, but can also allow the detection of analyte molecules with very low concentrations that cannot be detected under normal conditions.[30–32] To this end, molecular detection abilities of the platforms (two-arms in our case) were analyzed using MB solutions at different concentrations (10^{-3}–10^{-9} M). Here, the Raman spectra clearly showed that even very low concentrations, e.g., 10^{-9} M, could be detected with high signal-to-noise ratios by manipulating plasmonic hot-spot formations (Figure 4(III)).

In order to show the reason behind the enhancement in Raman intensity in two- and three-arms platform compared to the unfolded one, we performed finite difference time domain (FDTD) nearfield analyses for each configuration at the Raman laser excitation wavelength. **Figure 5**A shows the cross-sectional view of the electric field intensities showing the hot-spots with large local electromagnetic fields. A high and sensitive Raman signal requires strong light–matter interaction, which could be ensured with large local fields accessible to targeted materials on a plasmonic surface.[33] Comparing three configurations, we demonstrated that nearfield intensity increases from unfolded to three-arms platform. More importantly, for the unfolded platform, these large nearfields are localized in a small spot within the gap between particles (Figure S14, Supporting Information). On the other hand, with the tilted nature of the two-arms platform, hot-spot spreads within a wider volume between two particles, which yields stronger Raman intensities compared to the unfolded platform. As the three-arms platform has multiple gap positions, we used two field monitors in FDTD simulations as schematically shown in Figure 5A. First monitor locating between bottom particles and cutting through the top one demonstrates the local electromagnetic fields concentrated between two bottom gold particles with much larger intensities compared to the unfolded and two-arms platforms. The second monitor shows the two hot-spots excited within the gaps between the top and two bottom particles. These large nearfields are more accessible compared to the unfolded and two-arms platforms which enables three-arms platform to yield much larger Raman intensities in our experimental measurements. Figure 5B shows the maximum electric field intensities determined from FDTD simulations for the three configurations. Simulation results coincide well with the experiments, e.g., decreasing gap further enhances nearfield intensities, which increases the Raman intensity.

In the last part of our study, a proof-of-concept demonstration is performed using the fabricated platforms. At this point, our goal is to collect analyte molecules from a target point by controlling the motion of polymeric platforms and to perform SERS analysis in the desired environment following them. In order to control the motion of polymeric platforms (soft

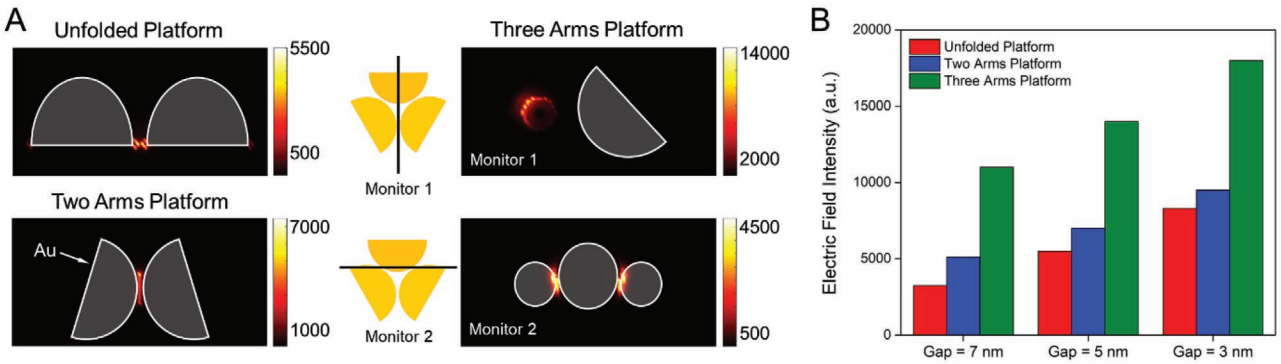

Figure 5. A) Cross-sectional nearfield intensity distributions calculated for unfolded, two- and three-arms platforms calculated via FDTD simulations. In the figure, the position of the two monitors used for the three arms platforms are schematically shown. B) Maximum electric field intensity enhancements determined for three configurations with different gap sizes.

actuators), they were decorated with a magnetic film (2 × 2 mm, 0.4 mm thickness) after design and fabrication. Magnetic films enable the motion of platforms with the help of a magnetic field. A cotton ball impregnated with 0.1 M MB molecules was used as a target, and the IR light source was chosen for folding the platforms. In the experiment, the two-arms actuator platform was first delivered to the target area by controlling the magnetic field and, analyte molecules from the target were transferred to the platforms with the swab using the light source (**Figure 6**a; Movie S3, Supporting

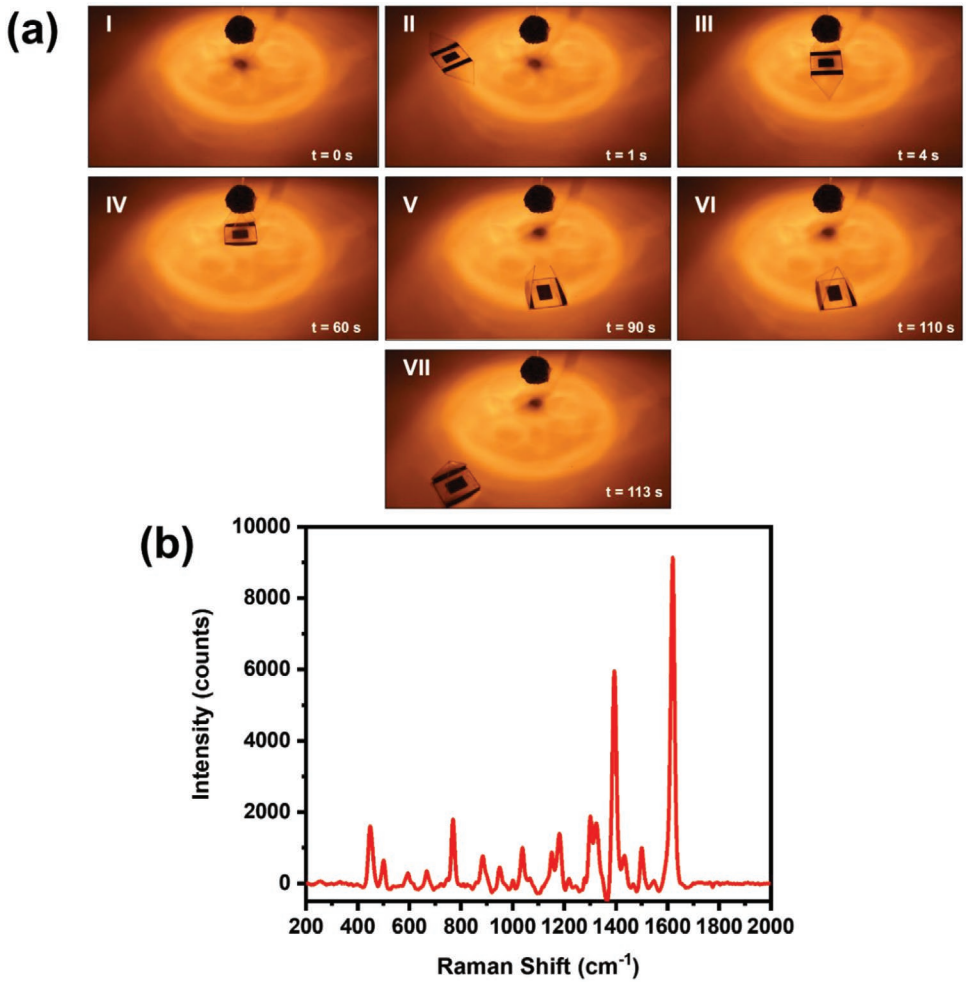

Figure 6. a) Optical images of magnet-powered motion and sample collection (swapping) from MB impregnated cotton ball using two-arms polymeric platforms. b) SERS spectrum of target molecules (MB in our case) collected using fabricated polymeric platforms.

Information). Folding of the platforms has been subsequently completed to maximize the formation of hot-spots on the platforms. Finally, the platforms were taken to the area where the SERS analysis were performed with the help of the magnetic field. The SERS spectrum shows that the target molecules could be successfully detected with the fabricated platforms (Figure 6b).

3. Conclusion

Thanks to their manipulation capabilities, soft actuators offer new possibilities in variety of technological areas where the plasmonic hot-spot formations play a key role. The polymer-based, easy to design actuator platforms introduced in this article were able to demonstrate a Raman signal enhancement as large as ≈70 folds only by controlling the folding of their arms. In addition, sample collection and analysis were successfully implemented through the magnetic field control of the platform motion and folding manipulation. The introduced soft actuators could be employed as next-generation Raman enhancement substrates as it brought new modalities, e.g., (i) The AuNP-decorated soft actuators simply allow to the enhancement of hot-spot formations with large local electromagnetic fields by controlling folding of their arms. Such manipulations are still challenging to perform with the traditional hot-spot engineering techniques due to high process cost, complexity, and inability of large-area fabrication. (ii) The ability to control the motion of the platforms by a magnetic field provides the sampling and analysis of target molecules. (iii) Surface of the platforms could also be decorated with other plasmonic nano-structures (e.g., star, rod, or 3D nanowire arrays) to further enhance its SERS ability. (iv) The platform could be designed into different geometries and sizes to analyze multiple targets. (v) Folding based hot-spot formations could also be triggered by a magnetic field, electrical stimulation, or pH which may expand the applicability of these platforms. Consequently, we believe that our observations could offer not only a new perspective to the design of the next-generation SERS platforms, but also provide an important advance in the applicability of SERS to the field of sensing.

4. Experimental Section

Fabrication of Platforms: The transparent pre-strained PS sheet (Grafix) with a thickness of 0.27 mm was used as a starting material. All polymeric patterns were designed in AutoCAD and printed on PS sheets using an HP Color LaserJet M553. Pattern dimensions of the platforms investigated for the controlled folding studies were described in in Figure S1 in the Supporting Information. The polymeric platforms were then obtained by cutting the PS sheets with a scalpel (No:11). In the experiments, 50 watt red (630 nm), blue (470 nm), and green (530 nm) LEDs, and 250 watt IR lamb were used as the light sources for folding of the polymeric platforms. In the folding investigations, 50 W LEDs were placed ≈2–3 cm away from the surface of the polymeric platforms, and a 250 W IR lamb was also placed ≈8 cm away from the surface of the platforms to obtain reasonable high energy intensity and leave sufficient space for the folding motion. Folding process of all samples was recorded by a Canon EOS 650D camera. The folding angles were then calculated via IMAGEJ software.

To modify polymeric platforms with plasmonic AuNPs, the two-and three-arms polymeric platforms were first immersed into a dopamine solution (dopamine hydrochloride (Sigma H8502), 2.0 mg mL^{-1} in 10×10^{-3} M Tris buffer, pH 8.5) at room temperature for 3 h. The samples were then rinsed with water and dried with N_2 gas. Finally, PDOP coated polymeric platforms were immersed into aqueous AuNP solution (1.71×10^{-9} M) for varying time intervals (3–24 h). The synthesis of AuNPs was given elsewhere.[34]

SERS Experiments: A Delta Nu Examiner Raman microscope with a 785 nm laser source was used for Raman studies with an operational range of 200–2000 cm^{-1}. Unless otherwise stated, all Raman measurements were performed under the same experimental conditions (i.e., ×20 microscope objective with a 3 µm laser spot size, 150 mW laser power, and 30 s acquisition time). To evaluate the SERS enhancement performance of the platforms, MB, a Raman probe, was drop-casted (5.0 µL, 10^{-3} M in water) and kept in a hood until dry. The Raman spectra were then obtained from at least ten different locations of the dried spot area for each sample. For folded platforms, Raman measurements were carried out at parallel direction as shown in Figure S11 in the Supporting Information. In order to calculate the LSPR modes via FDTD simulations (Lumerical Inc.), for the unit cell which consists of gold nanoparticles, perfectly matched layer boundary condition was used for all directions. Mesh size in all directions was chosen as 0.2 nm. Dielectric constant of gold was taken from Palik's Handbook of Optical Constants of Solids.[35]

Supporting Information

Supporting Information is available from the Wiley Online Library or from the author.

Conflict of Interest

The authors declare no conflict of interest.

Data Availability Statement

The data that support the findings of this study are available from the corresponding author upon reasonable request.

Keywords

hot-spot engineering, polymer folding, soft actuators, surface-enhanced Raman spectroscopy (SERS)

Received: January 3, 2021
Revised: April 12, 2021
Published online:

[1] Y. Song, P. Chen, M. T. Chung, R. Nidetz, Y. Park, Z. Liu, W. McHugh, T. T. Cornell, J. Fu, K. Kurabayashi, *Nano Lett.* **2017**, *17*, 2374.
[2] S. Chen, C. Liu, Y. Liu, Q. Liu, M. Lu, S. Bi, Z. Jing, Q. Yu, W. Peng, *Adv. Sci.* **2020**, *7*, 2000763.
[3] K. J. Freedman, L. M. Otto, A. P. Ivanov, A. Barik, S. H. Oh, J. B. Edel, *Nat. Commun.* **2016**, *7*, 10217.
[4] K. V. Sreekanth, S. Sreejith, Y. Alapan, M. Sitti, C. T. Lim, R. Sing, *Adv. Opt. Mater.* **2019**, *7*, 1801313.
[5] W. Li, L. Xiong, N. Li, S. Pang, G. Xu, C. Yi, Z. Wang, G. Gu, K. Li, W. Li, L. Wei, G. Li, C. Yang, M. Chen, *J. Mater. Chem. C* **2019**, *7*, 10179.

[6] T. M. Hwang, M. Heiranian, Y. Kim, S. You, J. Leem, A. Taqieddin, V. Faramarzi, Y. Jing, I. Park, A. M. van der Zande, S. Nam, N. R. Aluru, R. Bashir, *Nat. Commun.* **2020**, *11*, 1543.
[7] X. Wu, C. Hao, J. Kumar, H. Kuang, N. A. Kotov, L. M. Liz-Marzan, C. Xu, *Chem. Soc. Rev.* **2018**, *47*, 4677.
[8] A. Leitis, A. Tittl, M. Liu, B. H. Lee, M. B. Gu, Y. S. Kivshar, H. Altug, *Sci. Adv.* **2019**, *5*, eaaw2871.
[9] M. Fan, G. F. S. Andrade, A. G. A. Brolo, *Anal. Chim. Acta.* **2020**, *1097*, 1.
[10] G. Demirel, H. Usta, M. Yilmaz, M. Celik, H. A. Alidagi, F. Buyukserin, *J. Mater. Chem. C* **2018**, *6*, 5314.
[11] S. Y. Ding, J. Yi, J. F. Li, D. Y. Wu, R. Panneerselvam, Z. Q. Tian, *Nat. Rev. Mater.* **2016**, *1*, 16021.
[12] B. Yang, S. Jin, S. Guo, Y. Park, L. Chen, B. Zhao, Y. M. Jung, *ACS Omega* **2019**, *4*, 20101.
[13] G. Demirel, R. L. M. Gieseking, R. Ozdemir, S. Kahmann, M. A. Loi, G. C. Schatz, A. Facchetti, H. Usta, *Nat. Commun.* **2019**, *10*, 5502.
[14] M. Yilmaz, E. Babur, M. Ozdemir, R. L. Gieseking, Y. Dede, U. Tamer, G. C. Schatz, A. Facchetti, H. Usta, G. Demirel, *Nat. Mater.* **2017**, *16*, 918.
[15] S. Pang, T. Yang, L. He, *TrAC, Trends Anal. Chem.* **2016**, *85*, 73.
[16] D. Zhang, H. You, L. Yuan, R. Hao, T. Li, J. Fang, *Anal. Chem.* **2019**, *91*, 4687.
[17] V. Heleg-Shabtai, H. Sharabi, A. Zaltsman, I. Ron, A. Pevzner, *Analyst* **2020**, *145*, 6334.
[18] H. K. Lee, Y. H. Lee, C. S. L. Koh, G. C. Phan-Quang, X. Han, C. L. Lay, H. Y. F. Sim, Y. C. Kao, Q. An, X. Y. Ling, *Chem. Soc. Rev.* **2019**, *48*, 731.
[19] H. Y. Chen, M. H. Lin, C. Y. Yang, Y. M. Chang, S. Gwo, *J. Am. Chem. Soc.* **2015**, *137*, 13698.
[20] S. L. Kleinman, R. R. Frontiera, A. I. Henry, J. A. Dieringer, R. P. Van Duyne, *Phys. Chem. Chem. Phys.* **2013**, *15*, 21.
[21] Q. Jin, M. Li, B. Polat, S. K. Paidi, A. Dai, A. Zhang, J. V. Pagaduan, I. Barman, D. H. Gracias, *Angew. Chem., Int. Ed.* **2017**, *56*, 3822.
[22] W. Xu, S. K. Paidi, Z. Qin, Q. Huang, C. H. Yu, J. V. Pagaduan, M. J. Buehler, I. Barman, D. H. Gracias, *Nano Lett.* **2019**, *19*, 1409.
[23] Y. Liu, J. K. Boyles, J. Genzer, M. D. Dickey, *Soft Matter* **2012**, *8*, 1764.
[24] Y. Liu, B. Shaw, M. D. Dickey, J. Genzer, *Sci. Adv.* **2017**, *3*, e16022417.
[25] Y. Lee, H. Lee, T. Hwang, J. G. Lee, M. Cho, *Sci. Rep.* **2015**, *5*, 16544.
[26] H. Lee, S. M. Dellatore, W. M. Miller, P. B. Messersmith, *Science* **2007**, *318*, 426.
[27] T. G. Barclay, H. M. Hegab, S. R. Clarke, M. Ginic-Markovic, *Adv. Mater.* **2017**, *4*, 1601192.
[28] M. Yilmaz, G. Bakirci, H. Erdogan, U. Tamer, G. Demirel, *RSC Adv.* **2016**, *6*, 12638.
[29] M. S. Akin, M. Yilmaz, E. Babur, B. Ozdemir, H. Erdogan, U. Tamer, G. Demirel, *J. Mater. Chem. B* **2014**, *2*, 4894.
[30] G. C. Phan-Quang, H. K. Lee, I. Y. Phang, X. Y. Ling, *Angew. Chem., Int. Ed.* **2015**, *54*, 9691.
[31] X. Han, C. S. L. Koh, H. K. Lee, W. S. Chew, X. Y. Ling, *ACS Appl. Mater. Interfaces* **2017**, *9*, 39635.
[32] C. S. L. Koh, H. K. Lee, X. Han, H. Y. F. Sim, X. Y. Ling, *Chem. Commun.* **2018**, *54*, 2546.
[33] A. E. Cetin, D. Etezadi, H. Altug, *Adv. Opt. Mater.* **2014**, *2*, 866.
[34] N. R. Jana, L. Gearheart, C. J. Murphy, *Langmuir* **2001**, *17*, 6782.
[35] E. D. Palik, *Handbook of Optical Constant of Solids*, Academic, Orlando, USA **1985**.